Journal of the Korean Ceramic Society
Vol. 53, No. 6, pp. 712~718, 2016.

http://dx.doi.org/10.4191/kcers.2016.53.6.712

Effect of Li_3BO_3 Additive on Densification and Ion Conductivity of Garnet-Type $Li_7La_3Zr_2O_{12}$ Solid Electrolytes of All-Solid-State Lithium-Ion Batteries

Ran-Hee Shin*,*, Sam-Ick Son**, Sung-Min Lee*, Yoon Soo Han*, Yong Do Kim***, and Sung-Soo Ryu*,†**

**Engineering Ceramic Center, Korea Institute of Ceramic Engineering and Technology, Icheon 17303, Korea*
***Central Research Institute, Hyundai Motors, Uiwang 16082, Korea*
****Department of Materials Science & Engineering, Hanyang University, Seoul 04763, Korea*

(Received October 4, 2016; Revised October 28, 2016; Accepted October 28, 2016)

ABSTRACT

In this study, we investigate the effect of the Li_3BO_3 additive on the densification and ionic conductivity of garnet-type $Li_7La_3Zr_2O_{12}$ solid electrolytes for all-solid-state lithium batteries. We analyze their densification behavior with the addition of Li_3BO_3 in the range of 2-10 wt.% by dilatometer measurements and isothermal sintering. Dilatometry analysis reveals that the sintering of $Li_7La_3Zr_2O_{12}$-Li_3BO_3 composites is characterized by two stages, resulting in two peaks, which show a significant dependence on the Li_3BO_3 additive content, in the shrinkage rate curves. Sintered density and total ion conductivity of the system increases with increasing Li_3BO_3 content. After sintering at 1100°C for 8 h, the $Li_7La_3Zr_2O_{12}$-8 wt.% Li_3BO_3 composite shows a total ionic conductivity of 1.61×10^{-5} Scm^{-1}, while that of the pure $Li_7La_3Zr_2O_{12}$ is only 5.98×10^{-6} Scm^{-1}.

Key words : Li ion battery, Solid electrolyte, Sintering, Sintering additive, Ion conductivity

1. Introduction

At present, Li-ion batteries have several problems such as leakage of the liquid organic electrolyte and low thermal stability, which occasionally leads to explosions. These critical issues have brought our attention to the development of an all-solid-state Li-ion battery with high stability and reliability, along with high energy density. To achieve this goal, it is essential to replace the current liquid-phase electrolyte with a solid one of higher stability.[1,2] Solid electrolytes actively studied for this purpose mainly include oxide and sulfide materials, such as perovskites, titanates,[3-5] NASICON phosphates,[6-8] LISICON sulfides,[9,10] and garnet-structure oxides.[11-16] Among the latter, $Li_7La_3Zr_2O_{12}$ (LLZ) with a cubic or garnet structure has demonstrated promise, since it is inert against the Li electrode and stable both thermally and chemically.[13]

Depending on the temperature during thermal treatment, LLZ can be either tetragonal or cubic, with ionic conductivities higher than 10^{-6} Scm^{-1} and 10^{-4} Scm^{-1}, respectively.[14] Thus, it is desirable to have LLZ in a stable cubic form to achieve a higher ionic conductivity. Optimal densification is another important factor that can minimize resistance along grain boundaries. It is evident that the presence of pores left from an unsatisfactory sintering can reduce ionic movements, as well as degrade mechanical properties of the solid electrolyte.[17]

LLZ generally densifies at temperatures above 1200°C via solid-state sintering. This rather high sintering temperature, however, can cause volatilization of Li and lead to a phase transition. Therefore, for the purpose of this study it is required keep LLZ in a cubic form after densification at temperatures below 1200°C, and to maintain an enhanced ionic conductivity.[16] It is well known that the addition of a sintering additive of low melting temperature increases the efficiency of densification of solids, by providing a liquid-state sintering route for the system.

Known additives for LLZ densification include Li-containing ceramics such as Li_2O, $LiSiO_4$, and Li_3BO_3 (LBO).[18-23] Among these ceramics, LBO is reported to be highly effective for LLZ densification at low temperatures.[23] LBO forms a liquid phase during LLZ sintering at temperatures below 1000°C, and enhances the densification of LLZ grains via liquid-phase sintering. It also decreases the grain boundary resistance by forming thin layers on LLZ grains, thus increasing the ionic conductivity of LLZ.[18]

In this study, we used LBO as a sintering additive for the low-temperature sintering of LLZ. Dilatometric analysis was used to investigate the densification behavior of LLZ in terms of LBO content and to evaluate its sintering behavior at various temperatures. We analyzed the resultant microstructure development to determine the crystalline phase in terms of LBO content and sintering temperature, and also evaluated the ionic conductivity.

†Corresponding author : Sung-Soo Ryu
E-mail : ssryu@kicet.re.kr
Tel : +82-31-645-1447 Fax : +82-31-645-1485

2. Experimental Procedure

For the synthesis of the LLZ-LBO composites, commercial LLZ powder (mean particle size: 2.75 μm; purity: 99.9%, Schott, Germany) was used as the starting raw material, together with LBO powder (mean particle size: 5 μm; purity: 99.9%, Toshima, Japan) as the sintering additive. They were mixed in a Mini mill (Pulverisette 23, FRITSCH, Germany), and the mixture was formed into disc-type sample by pressing into a mold (dia. 10 mm) of super-alloy at 124 MPa, followed by cold-isostatic pressing at 200 MPa. These disc samples had densities in the range of 55±2% of the theoretical value.

The shrinkage behavior of the LLZ-LBO composites with different LBO contents was evaluated by heating the sample up to 1200°C at a constant heating rate of 5°C/min in air in a push-rod dilatometer (DIL-402C, NETZCH, Germany). The LLZ-LBO samples with different LBO contents were also subjected to isothermal sintering at 1100°C for 8 h in air. The powder compacts were covered with their parent powders in an Al_2O_3 crucible. To investigate the effect of temperature on the sintering of the LLZ-8 wt.% LBO composite, samples were sintered in the temperature range of 900 - 1200°C for 8 h at a heating rate of 5°C/min in air. For comparison purposes, an LLZ sample without any added LBO was also prepared and densified under identical conditions.

The density of the samples after sintering was determined from the weight and physical dimensions. The microstructure of the fractured surfaces of the sintered samples was observed by field emission scanning electron microscopy (FE-SEM, JSM-9701, JEOL, Japan). Furthermore, the crystalline phases of the sintered specimens were identified using X-ray diffractometry (XRD, RINT-2000, Rigaku Corp., Japan).

We measured the ionic conductivity of the sintered and polished LLZ-LBO bodies, which has a constant area (A) and thickness (l), using the following procedure. First, we coated both surfaces of each sample with a highly-conductive Au electrode by sputtering. Then, we measured its impedances with an impedance analyzer (Agilent 4192A, Hewlett Packard, USA) by applying an AC current of 0.05 V in the frequency range of 10-13 MHz. Resistance (R_b) of the electrolyte was obtained from the intercept of the measured half-circle trajectories of impedance with the real-part axis. Finally, the ionic conductivity (σ) was calculated by using the following formula:

$$\sigma\ (\Omega \cdot cm)^{-1} = \frac{1}{R_b} \cdot \frac{l}{A} \quad (1)$$

3. Results and Discussion

Figure 1 presents SEM images of the LLZ and LBO powders used in this study, which indicate that the LLZ particles have a size range of 1-3 μm with some local agglomerates, whereas the LBO is relatively homogeneous with a particle of 5 μm.

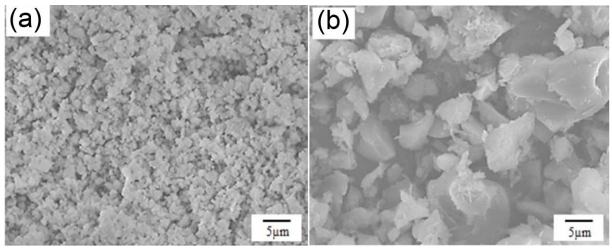

Fig. 1. SEM images for morphologies of starting materials: (a) LLZ powder and (b) LBO powder.

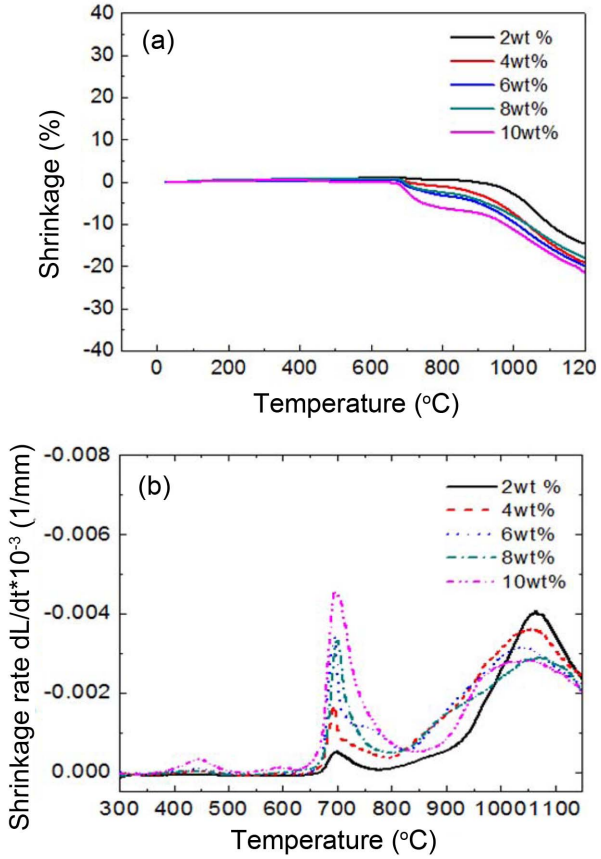

Fig. 2. Changes of (a) linear shrinkage and (b) linear shrinkage rate as a function of temperature for LLZ with different LBO additions sintered up to 1200°C.

Figure 2(a) shows the shrinkage behavior of the LLZ-LBO composites with various LBO contents obtained via dilatometry, which identifies the first shrinkage at approximately 700°C. Fig. 2(b) is a shrinkage rate graph, which clearly shows sintering in two stages, one around 700°C and another above 1000°C.

We interpret this observation as two different sintering mechanisms being involved in the sintering of the LLZ-LBO composites, depending on the temperature. The first one at around 700°C is apparently due to the viscous flow of LBO glass once its viscosity becomes low enough. The second one is likely due to liquid-phase sintering by LBO that melts at

850°C, which leads to rearrangement and solid-state sintering of LLZ grains.[24] Although the melting point of LBO glass is known to be around 700°C,[21] this study shows that liquid-phase sintering becomes active around 850°C.

As shown in Fig. 2(a), the shrinkage behavior of the LLZ-LBO composite strongly depends on LBO content. As LBO content is increased, LLZ shrinkage increases. The shrinkage rate, as shown in Fig. 2(b) indicates that the first peak due to viscous sintering of LBO takes place at the same temperature independent of LBO content. However, the increase in LBO content increases the peak intensity. The second peak above 900°C has a tendency move to lower temperatures with increasing LBO content. These observations suggest that increasing LBO content intensifies its role in the densification of LLZ.

Figure 3(a) and 3(b) summarize the apparent and relative densities of the sintered LLZ-LBO composites with varying LBO contents at 1100°C. The density of pure, sintered LLZ is 2.98 gcm^{-3}, and it increases with the addition of LBO. Here, we assumed that varying the LBO content changes the theoretical density of the LLZ-LBO composites, and estimated all densities using the theoretical densities of LLZ (ρ_{LLZ}: 5.11 gcm^{-3}) and LBO (ρ_{LBO}: 2.16 gcm^{-3}) as starting points.

This effect of LBO is attributed to a more uniformly-distributed LBO liquid on the LLZ grains at higher LBO contents, which certainly leads to an enhanced densification. The highest relative density of the sintered composite is 77%, at LBO contents above 8 wt.%. This is a marked enhancement compared to the 58% density of pure LLZ. However, a sintered density of 77% is still somewhat lower than other reported results,[23] which suggests that further research may be needed in this respect.

Figure 4 presents the XRD patterns of the LLZ-LBO composites with different LBO contents after sintering at 1100°C, and clearly shows the main LLZ cubic garnet phase. Note that a strong peak corresponding to the $La_2Zr_2O_7$ (LZ) pyrochlore phase appears in the LLZ sample which does not have added LBO. The presence of a pyrochlore phase is attributed to the volatilization of Li_2O, which makes the LZ phase more stable thermodynamically.[25] The peak intensity of the LZ phase decreases with increasing LBO content, and eventually disappears, leaving only the cubic LLZ phase when the LBO content is higher than 8 wt.%.

We conclude that LBO plays a critical role in suppressing Li_2O volatilization from LLZ, thus stabilizing the cubic structure. None of the LLZ samples with LBO show an LBO-containing crystalline phase, which indicates that LBO does not interact with LLZ to form a new crystalline phase. Therefore, the LBO must remain on the grain boundary of LLZ as an amorphous state.[18]

Figure 5 gives the microstructural images of the fractured surfaces of the LLZ samples with varying LBO contents sin-

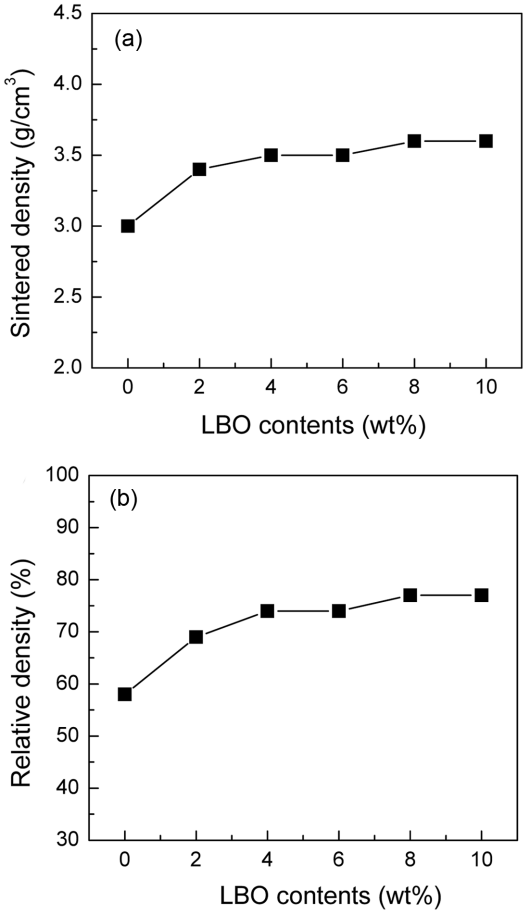

Fig. 3. (a) Sintered densities and (b) relative densities of the LLZ samples with various contents of LBO additive sintered at 1100°C for 8 h in air.

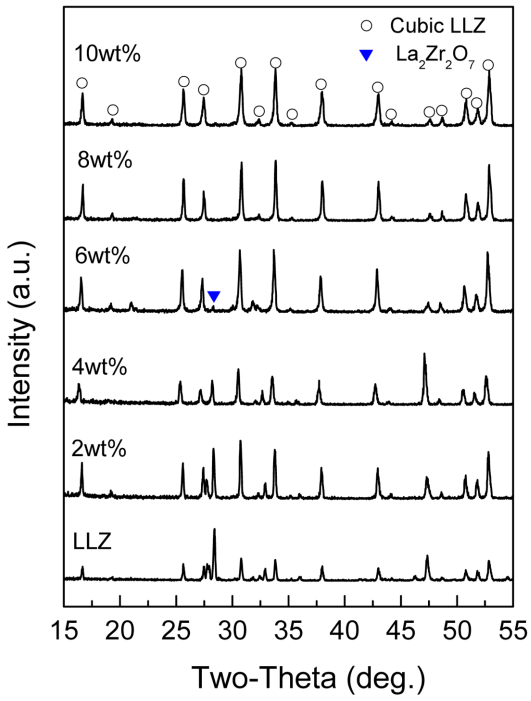

Fig. 4. XRD patterns for the LLZ samples with various LBO additions in the range of 0 to 10 wt.% , which are sintered at 1100°C for 8 h in air.

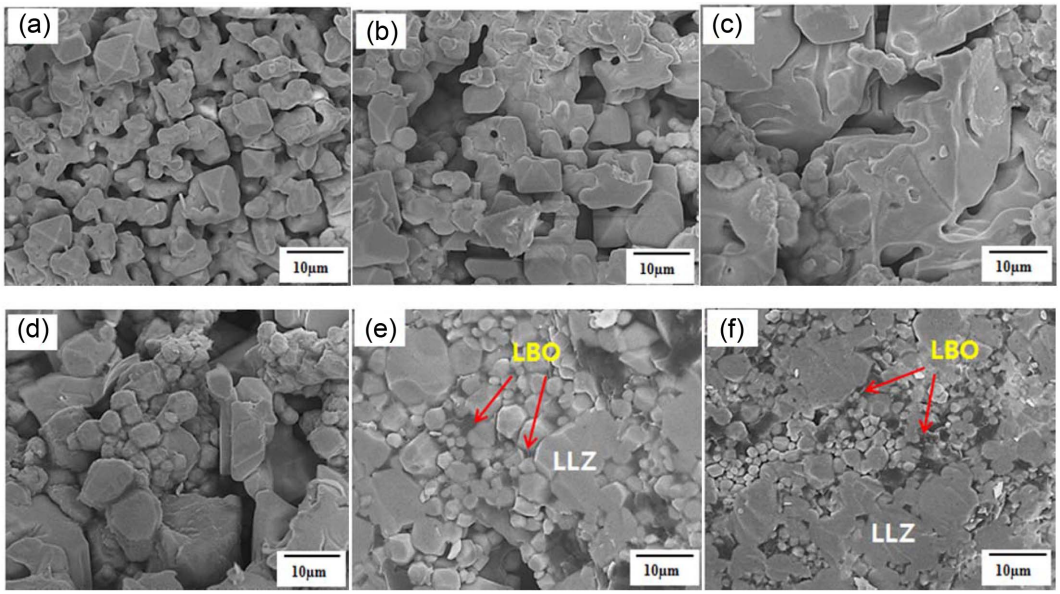

Fig. 5. FE-SEM images for fractured surfaces of the LLZ-LBO composites with different LBO contents sintered at 1100 °C for 8 h in air; (a) pure LLZ, (b) 2 wt.% LBO, (c) 4 wt.% LBO, (d) 6 wt.% LBO, (e) 8 wt.% LBO, and (f) 10 wt.% LBO.

tered at 1100°C for 8 h, obtained by FE-SEM. The pure LLZ shows many pores on the grain boundaries, while the composites with LBO show progressively denser microstructures. Up to the LBO content of 6 wt.%, liquid LBO is present only locally along with many pores. Above the LBO content of 8 wt.%, liquid LBO is distributed rather uniformly on grain boundaries, and a dense microstructure with markedly decreased pore numbers becomes evident.

In addition, we notice a significant growth in the LLZ grains with LBO addition, compared to pure LLZ. This is in agreement with the shrinkage behavior in Fig. 2, which shows that the densification of the LBO-added LLZ proceeds via both melted LBO and solid-state LLZ grains, which eventually leads to grain growth. We also observe some LLZ grains to grow abnormally (bigger than 10 μm). We currently attribute this behavior to the powder characteristic of the LLZ raw material, which can be verified by future investigations.

Figure 6 plots the density of the LLZ-8 wt.% LBO composite sintered for 8 h at various sintering temperatures. The pure LLZ shows a low relative density of 57% at 900°C, and increases its value with rising temperatures, reaching 74% at 1200°C. The LLZ-8 wt.% LBO composite, however, reaches a relative density of 66% at 900°C. Although this density is higher than that of the pure LLZ, it is comparatively low considering that the temperature is already higher than the melting point of LBO.

For the composites, an increase in temperature also results in higher densities up to 77% at 1100°C. We thus confirm that the LLZ-LBO composites sinter by two mechanisms, one via the liquid-phase sintering due to melted LBO, and another via the solid-state sintering of LLZ grains. At 1200°C, the LLZ-8 wt.% LBO composite shows a

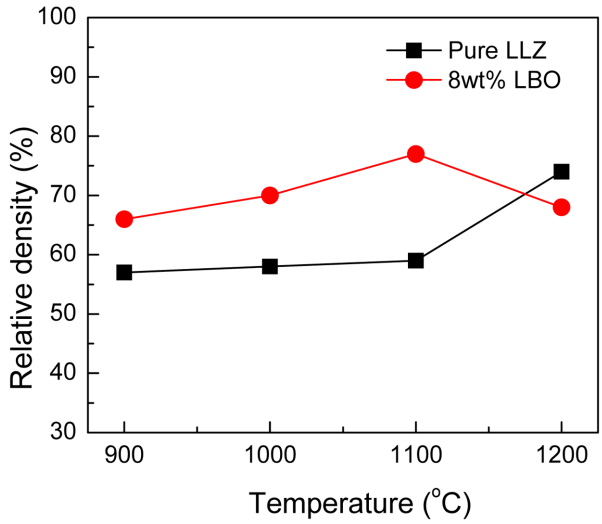

Fig. 6. Relative sintered density as a function of temperature for pure LLZ and LLZ-8 wt.% LBO specimens, which were sintered for 8 h in air.

drastic decrease in sintered density, and becomes less dense than the pure LLZ. We assume that this could be due either to the formation of a secondary phase from the interaction between LLZ and LBO during liquid-phase sintering at higher temperatures, or to the loss of Li and B components from the sintering additive by volatilization.

To confirm which mechanism is actually taking place, we carried out further phase analyses on the sintered bodies by XRD. Fig. 7 depicts the XRD patterns of the LLZ-8 wt.% LBO composite at various sintering temperatures. It shows peaks of only the cubic LLZ phase up to a sintering temperature of 1100°C. With increasing temperature, the inten-

sity of the cubic LLZ phase increases. At 1200°C, however, the cubic LLZ peaks disappear, and only the LZ pyrochlore peaks remain. We assume that this is due to the decomposition of both LLZ and LBO at a high temperature of 1200°C, followed by volatilization of the decomposed Li and B.

Figure 8 contains FE-SEM images of the LLZ-8 wt.% LBO composites, which were sintered at various temperatures and fractured to conduct the microstructural observations. With increasing temperature, the LLZ exhibits densification accompanied by grain growth. When LBO is added as a sintering additive, increase in sintering temperature provides the coupled densification routes; one via rearrangement of LLZ grains by liquid-phase sintering and another by grain growth of LLZ grains by solid-state sintering. At temperatures of 900°C and 1000°C, LBO is not distributed uniformly and a large area is occupied by pores, and no sintering between LLZ grains is observed. The densest microstructure is observed in the sample sintered at 1100°C. In accordance with the XRD analysis, the sample sintered at 1200°C shows a completely different microstructure compared to samples sintered at temperatures below 1100°C, owing to the presence of only the LZ phase after losses of Li and B.

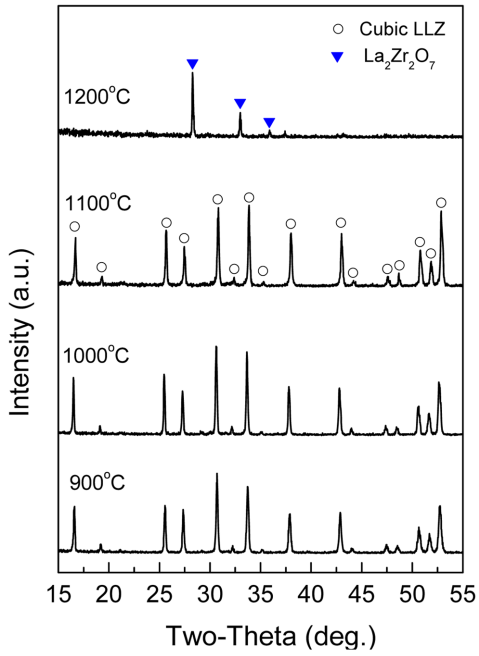

Fig. 7. XRD patterns as a function of sintering temperature for the LLZ sample with 8 wt.% LBO addition. Sintering was carried out for 8 h in air.

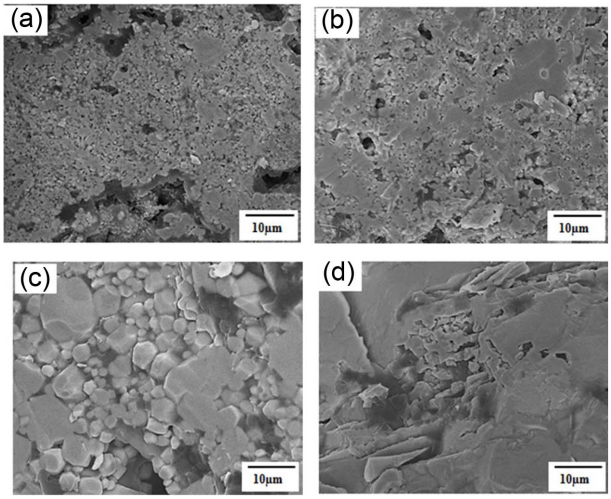

Fig. 8. FE-SEM images of the fractured LLZ samples with 8 wt.% LBO addition sintered for 8 h at different temperatures; (a) 900°C, (b) 1000°C, (c) 1100°C, and (d) 1200°C.

Figure 9 is the plot of the impedance of the LLZ-LBO composites measured at 28°C as a function of their LBO content. The sintered LLZ bodies containing LBO have many resistance elements such as the LLZ bulk, LBO bulk, LLZ/LLZ grain boundaries, and LLZ/LBO interfaces. It is however not easy to treat each element separately, and the ionic conductivity given here is the measured total value.[18] Thus, the overall resistance of the sample was determined from the intersection of the semicircle with the real part of the impedance (abscissa). As shown in Fig. 9, the pure LLZ sample has an impedance function with two semicircles, one due to grains at the frequency range of 13 MHz-5 kHz, and another due to grain boundaries at the frequency range of 5.0 - 0.7 kHz. We confirm that the increase in LBO content enhances ionic conductivity and reduces the grain boundary resistance, apparently due to the presence of the uniformly distributed LBO phase on the LLZ grain boundaries. Using the resistance values from the impedance plot, ionic conductivities are calculated by Eq. (1), and tabulated in Table 1 in terms of LBO content. The pure LLZ shows a total ionic conductivity of 5.98×10^{-6} Scm^{-1}. As the LBO content increases, ionic conductivities of the LLZ samples increase, reaching 1.61×10^{-5} Scm^{-1} at 8 wt.% LBO addition, which is much

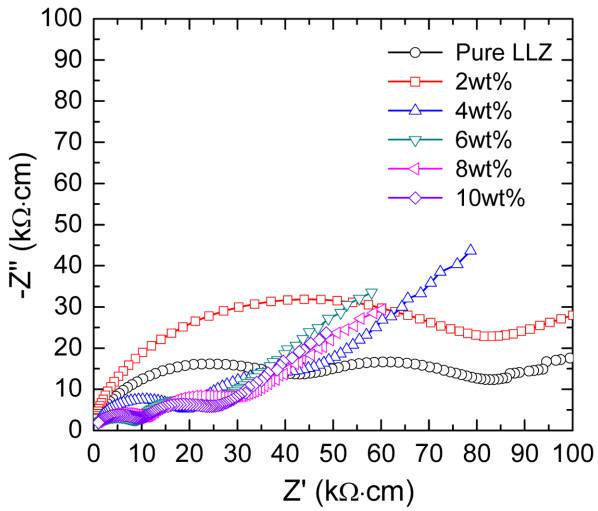

Fig. 9. Impedance spectra at 28°C for the LLZ specimens with different LBO contents, which was sintered at 1100°C for 8 h in air.

Table 1. Relative sintered density and total Li-ion conductivity of the LLZ sample with different LBO contents

LBO contents (wt.%)	Relative density (%)	Total ionic conductivity (S/cm^{-1})
0	58	5.98×10^{-6}
2	69	6.24×10^{-6}
4	74	8.95×10^{-6}
6	74	1.55×10^{-5}
8	77	1.61×10^{-5}
10	76	1.56×10^{-5}

greater than that of the pure LLZ sample.

According to the study by Rosero-Navarro et al.,[23] for $Li_7La_3(Zr_{2-x}Nb_x)O_{12}$ with 6.5% LBO added, the sintered density was 86% of the theoretical, and its ionic conductivity was 7×10^{-5} Scm^{-1}. Compared to this result, the LLZ-8wt.% LBO sample in this study shows a somewhat lower ionic conductivity, which is presumably due to its lower density. In addition, characteristics of the LLZ raw material such as grain size, uniformity, and the presence of dopants such as Al, Zr, and Nb may affect its properties.

Figure 10 gives the impedance spectra of the LLZ-8 wt.% LBO composites measured at 28°C as a function of sintering temperature, and shows that the ionic conductivity increases when sintering temperature increases. Total ionic conductivities are calculated to be 3.33×10^{-6} Scm^{-1} and 1.61×10^{-5} Scm^{-1} at 1000°C and 1100°C, respectively. At 1200°C, on the other hand, the change in crystal structure increases the overall resistance, and makes it impossible to distinguish the bulk and grain boundary impedances. From these results, we confirm that higher densification reduces the grain boundary resistance and enhances the ionic conductivity of the composites.

4. Conclusions

In this study, we prepared the garnet-type LLZ solid electrolyte with the addition of LBO as a sintering aid, and investigated its densification behavior and ionic conductivity. Shrinkage behavior of the LLZ-LBO composites at various LBO concentrations, determined via dilatometry analysis, showed that their sintering takes place in two stages, the first around 700°C and the second above 800°C. Increasing LBO content increased the effect of LBO on the densification of LLZ. Sintered density increased with increasing LBO addition, reaching a maximum value of 77% at an LBO concentration of 8 wt.%, which is a marked increase compared to the 58% of the pure LLZ. Using XRD analysis, we further confirmed that increasing LBO content suppressed the formation of a secondary $La_2Zr_2O_7$ phase in the LLZ samples, and eventually formed a stable cubic LLZ structure at LBO additions above 8 wt.%. Increasing LBO content also enhanced ionic conductivity and reduced grain boundary resistance, resulting in an ionic conductivity of 1.61×10^{-5} Scm^{-1} for the sample with 8 wt.% LBO.

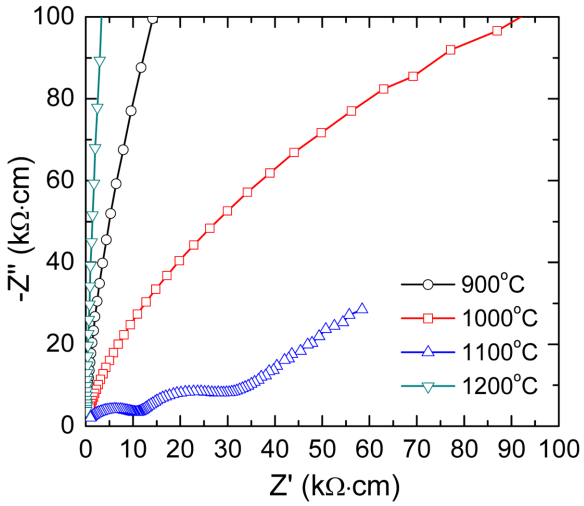

Fig. 10. Impedance spectra at 28°C as a function of sintering temperature for the LLZ samples with 8 wt.% LBO addition. Sintering were carried out for 8 h in air.

The LLZ-8 wt.% LBO composite showed the highest sintered density at 1100°C. However, it formed a cubic $La_2Zr_2O_7$ phase at 1200°C due to the volatilization of Li and B from the system. Ionic conductivities generally increased with increasing sintering temperature. Although we confirmed the above conclusions in this study, further investigations are needed to achieve improvements in the system through the refinement of the LLZ powder and more detailed optimizations of the sintering conditions.

REFERENCES

1. P. Knauth, "Inorganic Solid Li Ion Conductors: An Overview," *Solid State Ionics*, **180** [14-16] 911-16 (2009).
2. J. W. Fergus, "Ceramic and Polymeric Solid Electrolytes for Lithium-ion Batteries," *J. Power Sources,* **195** [15] 4554-69 (2010).
3. Y. Inaguma, L.Q. Chen, M. Itoh, T. Nakamura, T. Uchida, H. Ikuta, and M. Wakihara, "High Ionic Conductivity in Lithium Lanthanum Titanate," *Solid State Commun.,* **86** [10] 689-93 (1993).
4. Y. Inaguma, L. Q. Chen, M. Itoh, and T. Nakamura, "Candidate Compounds with Perovskite Structure for High Lithium Ionic Conductivity," *Solid State Ionics*, **70** 196-202 (1994).
5. G. Y. Adachi, N. Imanaka, and H. Aono, "Fast Li-circle Plus Conducting Ceramic Electrolytes," *Adv. Mater.*, **8** [2] 127-35 (1996).
6. H. Aono, E. Sugimoto, Y. Sadaoka, N. Imanaka, and G. Y. Adachi, "Ionic Conductivity of the Lithium Titanium Phosphate(Li1+xMXTi$_2$-x(PO$_4$)$_3$,M=Al, Sc, Y, and La) Systems," *J. Electrochem. Soc.*, **136** [2] 590-91 (1989).
7. K. Arbi, J. M. Rojo, and J. Sanz, "Lithium Mobility in Titanium based NASICON Li1+xTi$_2$-xAlx(PO$_4$)$_3$ and LiTi$_2$-xZr x(PO$_4$)$_3$ Materials Followed by NMR and Impedance Spectroscopy," *J. Eur. Ceram. Soc.,* **27** [13] 4215-18 (2007).

8. H. Aono, E. Sugimoto, Y. Sadaoka, N. Imanaka, and G. Adachi, "Electrical Property and Sinterability of $LiTi_2(PO4)_3$ Mixed with Lithium Salt (Li_3PO_4 or Li_3BO_3)," *Solid State Ionics*, **47** [3-4] 257-64 (1991) .
9. R. Kanno, T. Hata, Y. Kawamoto, and M. Irie, "Synthesis of a New Lithium Ionic Conductor, Thio-LISICON-lithium Germanium Sulfide System," *Solid State Ionics*, **130** [1-2] 97-104 (2000).
10. M. Murayama, R. Kanno, M. Irie, S. Ito, T. Hata, N. Sonoyama, and Y. Kawamoto, "Synthesis of a New Lithium Ionic Conductor, Thio-LISICON-lithium Silicon Sulfide System," *J. Solid State Chem*., **168** [1] 140-48 (2002).
11. V. Thangadurai, H. Kaack, and W. J. F. Weppner, "Novel Fast Lithium Ion Conduction in Garnet-type $Li_5La_3M_2O_{12}$ (M=NB, Ta)," *J. Am. Ceram. Soc*., **86** [3] 437-40 (2003).
12. V. Thangadurai, and W. J. F. Weppner, "$Li_6ALa_2Ta_2O_{12}$ (A = Sr, Ba): Novel Garnet-like Oxides for Fast Lithium Ion Conduction," *Adv. Funct. Mater*., **15** [1] 107-12 (2005).
13. R. Murugan, W. Weppner, P. Schmid-Beurmann, and V. Thangadurai, "Structure and Lithium Ion Conductivity of Garnet-like $Li_5La_3Sb_2O_{12}$ and $Li_6SrLa_2Sb_2O_{12}$," *Mater. Res. Bull*., **43** [10] 2579-91 (2008).
14. R. Murugan, V. Thangadurai, and W. Weppner, "Fast Lithium Ion Conduction in Garnet-type $Li_7La_3Zr_2O_{12}$," *Angew. Chem. Int. Ed.*, **46** [41] 7778-81 (2007).
15. E. J. Cussen, "The Structure of Lithium Garnets: Cation Disorder and Clustering in a New Family of Fast Li+ Conductors," *Chem. Commun*., **37** [4] 412-13 (2006).
16. M. Huang, T. Liu, Y. Deng, H. Geng, Y. Shen, Y. Lin, and W. Nan, "Effect of Sintering Temperature on Structure and Ionic Conductivity of Li_7-x$La_3Zr_2O_{12}$–0.5x (x = 0.5 ~ 0.7) Ceramics," *Solid State Ionics*, **204** [1] 41-5 (2011).
17. Y.-H. Cho, J. Wolfenstine, E. Rangasamy, H. Kim, H. Choe, and J. Sakamoto, "Mechanical Properties of the Solid Electrolyte: $Li_{0.33}La_{0.57}TiO_3$," *J. Mater. Sci*., **47** [16] 5970-77 (2012).
18. K. Tadanaga, R. Takano, T. Ichinose, S. Mori, A. Hayashi, and M. Tatsumisago, "Low Temperature Synthesis of Highly Ion Conductive $Li_7La_3Zr_2O_{12}$– Li_3BO_3 Composites," *Electrochem. Commun.,* **33** 51-4 (2013).
19. R. Takano, K. Tadanaga, A. Hayashi, and M. Tatsumisago, "Low Temperature Synthesis of Al-doped $Li_7La_3Zr_2O_{12}$ Solid Electrolyte by a Sol–gel Process," *Solid State Ionics*, **255** [1] 104-7 (2014).
20. S. Ohta, S. Komagata, J. Seki, T. Saeki, S. Morishita, and T. Asaoka, "All-solid-state Lithium Ion Battery Using Garnet-type Oxide and Li_3BO_3 Solid Electrolytes Fabricated by Screen-printing," *J. Power Sources*, **238** 53-6 (2013).
21. N. Janani, C. Deviannapoorani, L. Dhivya, and R. Murugan, "Influence of Sintering Additives on Densification and Li+ Conductivity of Al doped $Li_7La_3Zr_2O_{12}$ Lithium Garnet," *RSC Adv*., **4** [93] 51228-38 (2014).
22. Y. Li, Y. Cao, and X. Guo, "Influence of Lithium Oxide Additives on Densification and Ionic Conductivity of Garnet-type $Li_{6.75}La_3Zr_{1.75}Ta_{0.25}O_{12}$ Solid Electrolytes," *Solid State Ionics,* **253** [1] 76-80 (2013).
23. N. C. Rosero-Navarro, T. Yamashita, A. Miura, M. Higuchi, and K. Tadanaga, "Preparation of $Li_7La_3(Zr_2$-x, Nbx)O_{12} (x = 0-1.5) and $Li_3BO_3/LiBO_2$ Composites at Low Temperatures Using a Sol-gel Process," *Solid State Ionics*, **285** 6-12 (2016).
24. R. H. Shin, S. I. Son, Y. S. Han, Y. D. Kim, H. T. Kim, S. S. Ryu, and W. Pan, "Sintering Behavior of Garnet-type $Li_7La_3Zr_2O_{12}$-Li_3BO_3 Composite Solid Electrolytes for All-solid-state lithium Batteries," *Solid State Ionics,* submitted.
25. S. W. Baek, J. M. Lee, T. Y. Kim, M. S. Song, and Y. Park, "Garnet Related Lithium Ion Conductor Processed by Spark Plasma Sintering for All Solid State Batteries," *J. Power Sources,* **249** 197-206 (2014).